The Mechanism Controlling Static Liquefaction and Cyclic Strength of Sand

Ibsen, Lars Bo

Publication date:
1998

Document Version
Publisher's PDF, also known as Version of record

AAU Geotechnical Engineering Papers ISSN 1398-6465 R 9816

The mechanism controlling static liquefaction and cyclic strength of sand

L.B. Ibsen

1998 Soil Mechanics Paper No 27

GEOTECHNICAL ENGINEERING GROUP
AALBORG UNIVERSITY DENMARK

Ibsen, L.B. (1998). The mechanism controlling static liquefaction and cyclic strength of sand.

AAU Geotechnical Engineering Papers, ISSN 1398-6465 R9816.

Soil Mechanics Paper No 27

The paper has been published in *Proc.Int. Workshop on Physics and Mechanics of Soil Liquefaction, Baltimore. A.A. Balkema, ISBN 9058090388, pp. 29-39.*

The **A**AU **G**eotechnical **E**ngineering **P**apers - AGEP - are issued for early dissemination and book keeping of research results from the Geotechnical Engineering Group at Aalborg University (Department of Civil Engineering). Moreover, the papers accommodate proliferation and documentation of field and laboratory test series not directly suited for publication in journals or proceedings.

The papers are numbered ISSN 1398-6465 R<two digit year code><two digit consecutive number>. For internal purposes the papers are, further, submitted with coloured covers in the following series:

Series	Colour
Laboratory testing papers	sand
Field testing papers	grey
Manuals & guides	red
Soil Mechanics papers	blue
Foundation Engineering papers	green
Engineering Geology papers	yellow
Environmental Engineering papers	brown

In general the AGEP papers are submitted to journals, conferences or scientific meetings and hence, whenever possible, reference should be given to the final publication (journal, proceeding etc.) and not to the AGEPpaper.

Proc. of Int. Workshop on Physics and Mechanics of Soil Liquefaction, Baltimore, Sept. 1998.
To be published in A.A. Balkema.

The Mechanism Controlling Static Liquefaction and Cyclic Strength of Sand

L.B.Ibsen

Aalborg University, Denmark

ABSTRACT: Liquefaction and the cyclic strength of sand in undrained condition are strongly attached to the mechanisms observed in static tests. The cyclic failure condition, such as Cyclic Liquefaction and Cyclic Mobility is only part of the complex mechanism, which has to be determined in order to describe the development of stress and strain in cyclic tests. The key to explain and quantify the soil response is to understand the role of the volume changes and to be able to model these correctly. It is shown that the volume changes in soil subjected to static and cyclic loading are controlled by the characteristic line. Experiments have been performed to study the factors that influence the location of the characteristic line in drained and undrained tests for various types of sand and various types of loading. The relation of the characteristic line to other features of static, cyclic soil behaviour is explained and illustrated with experimental data.

1 INTRODUCTION

Liquefaction and the cyclic strength of sand in undrained conditions are strongly attached to the mechanisms observed in static tests. The cyclic failure condition, such as Cyclic Liquefaction and Cyclic Mobility is only part of the complex mechanism, which has to be determined in order to describe the development of stress and strain in cyclic tests. The paper will describe a number of new characteristic phenomena of dense sand subjected to cyclic loading, which have been observed in triaxial tests using specimens with equal height and diameter. Experiments have been performed to study the factors that influence and control the fatigue which leads to Static and Cyclic Liquefaction. These experiments have shown that it is the volume changes that is the key player for understanding the behaviour of soils whether under drained or undrained conditions. Volume changes can be compressive or expansive in nature. Expansive or dilative volume changes are most pronounced for dense sands at low confining pressures and high stress levels approaching failure. The transition from compressive behaviour observed at lower stress levels to dilative behaviour at high stress levels occurs along a straight line through the origin of the stress space. For drained tests, this line is referred to as the Characteristic line.

In elasto-plasticity models the Characteristic line, evaluated from $p' = const$ tests, corresponds to the point on the plastic potential surface where the plastic strain increment vector is perpendicular to the p'- axis or the hydrostatic axis. This state is therefore comparable to the similar point on the yield surface at which the normal is perpendicular to the hydrostatic axis. This indicates the point at which sand may become unstable, as explained in detail elsewhere (Lade 1995). Thus, the Characteristic line plays a similarly important role for the plastic potential surface as the instability line plays for the yield surface. Both lines are shown on the diagram in Figure 1. The behaviour of soils, static or cyclic is greatly influenced by and can be explained in view of the relative locations of these two lines. For sands the two lines are distinctly separate, while for normally consolidated, insensitive clays the two lines coincide, and they also coincide with the critical state or ultimate state line.

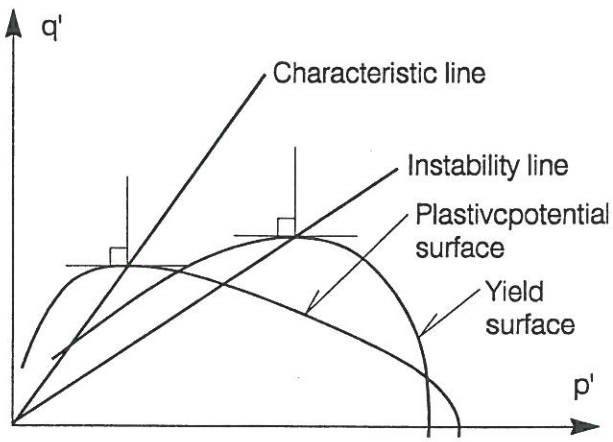

Figure 1. Characteristic and instability lines.

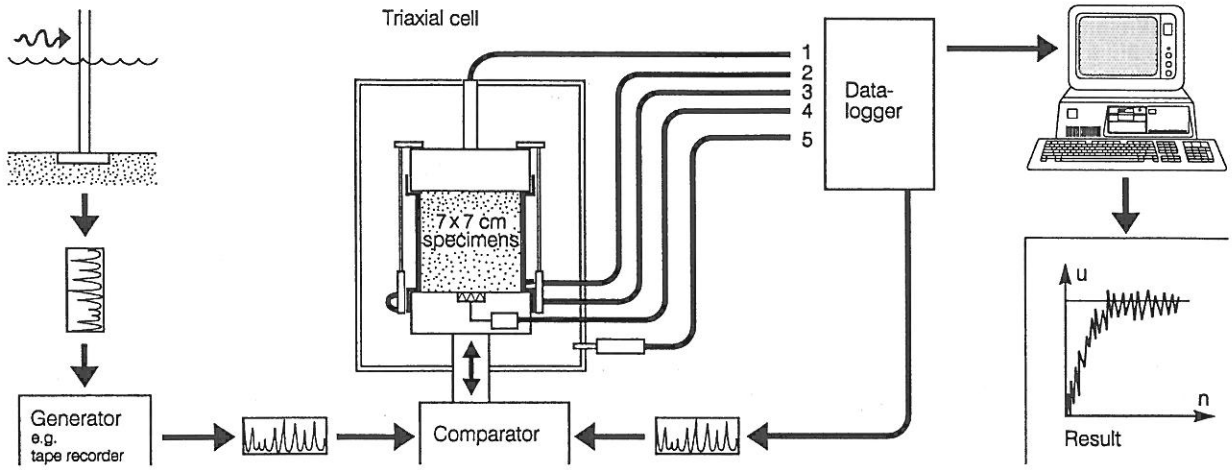

Figure 2. The principle of the Danish triaxial apparatus. It is fully automatic and run by a computer. The triaxial is constructed in agreement with the principles described in (Jacobsen, M. 1970)

2 EXPERIMENTAL METHODS

The tests performed in connection which this paper were conventional static CD-tests, CU-tests, $CU_{u=0}$-tests, and cyclic CU-tests. The cyclic tests were performed as undrained tests with pore pressure measurements. The $CU_{u=0}$-tests were carried out by measuring the volume change and controlling the cell pressure in such a way that $\delta\varepsilon_v = 0$ throughout the test. In this way the undrained condition is ensured and the effective stress path is followed throughout the test.

2.1 Testing equipment and procedures

To ensure homogeneous stress and strain conditions, the tests presented here were performed on cylindrical specimens with a height and diameter equal to 70 mm. Fully lubricated ends were employed on all test specimens. The lubricated ends consisted of latex rubber disks of 0.3 mm thickness placed onto the caps and bases of the specimen over a thin layer of vacuum grease. The tests were performed in a newly developed version of the Danish Triaxial Apparatus in which control of stress path, measurement, and data analysis is automated (Ibsen 1994). The apparatus is outlined in Figure 2.

The static triaxial specimen was loaded by a mechanically controlled piston, while the cyclic test is loaded by a hydraulic piston. The tests were performed with constant deformation rate of 4 % per hour. The measuring systems in the two apparatuses were identical and consisted of electronic load, pressure, and deformation transducers. The working principles of the triaxial cell are similar to those described by Jacobsen (1970).

2.2 Sand used

The study described in this paper is based on tests performed on two uniform sands: Aalborg University sand No. 1 and Lund sand No 0. The index properties for these sands are shown in Table 1.

Table 1. Index Properties.

Property	Aalborg University sand No 1	Lund sand No 0
$d_{50\ mm}$	0.14	0.4
C_U	1.78	1.7
d_s	2.65	2.65
e_{max}	0.86	0.82
e_{min}	0.55	0.55

2.3 Specimen preparation and saturation

The test specimens were prepared by a pluvial deposition and carefully saturated in total vacuum (approx. -98 kPa). This causes all specimens to be pre-consolidated to approximated 100 kPa during the preparation process. This technique ensures homogeneous and totally saturated specimens. The triaxial test series was performed on isotropically consolidated specimens with relative densities as shown in Table 2. The test results are reported by Ibsen, L.B (1993), Ibsen, L.B. and Bødker, L (1994), Jacobsen, F.R. and Simonsen, J (1994), and Ibsen and Jacobsen (1996).

Table 2. Relative densities for sand specimens in static triaxial tests.

	Relative densities
Aalborg University sand No. 1	0.10, 0.51, 0.80, 1.00
Lund sand No. 0	0.48, 0.78, 0.93, 1.00

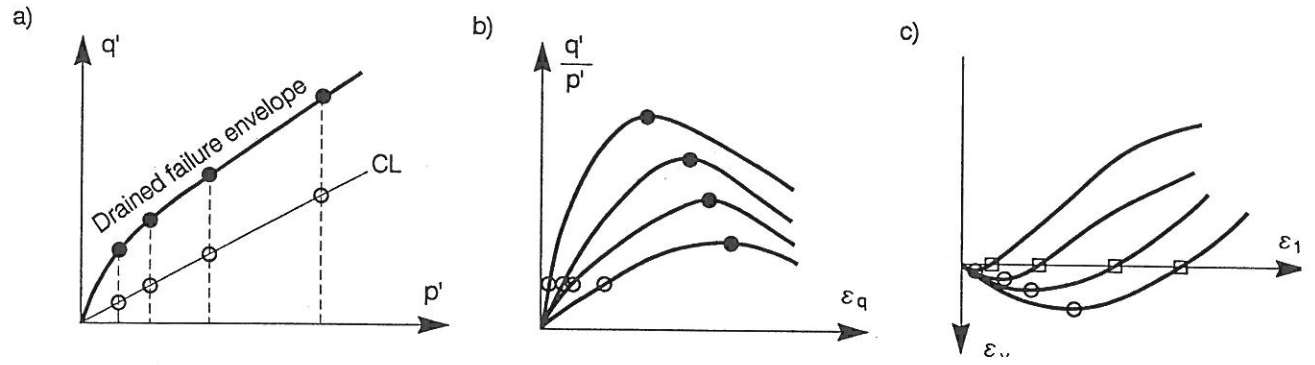

Figure 3. Diagram illustrating the development of stress-strain behaviour in drained triaxial compression tests on dense sand and specimens with equal height and diameter.

3 THE CHARACTERISTIC STATE

3.1 Definition of characteristic state

Figure 3 shows the results of four drained triaxial compression tests with the same initial density. The effective stress path is shown in Figure 3.a on a Cambridge diagram. The tests are performed with different initial mean normal pressures p', which are held constant throughout each test. Laboratory tests on several sands, (Lade and Ibsen 1997, Ibsen and Lade 1998) have shown that a characteristic threshold exists in granular materials which is defined as the stress state where the volume change goes from contraction to dilation. On the $\varepsilon_1 - \varepsilon_v$ curve, Figure 3.c, the characteristic threshold is marked by open circles at the point where the specimen has minimum volume. The stress state characterised by (p'_{cl}, q'_{cl}) where $\delta\varepsilon_v/\delta\varepsilon_1 = 0$ is defined and described as the *Characteristic State.* Characteristic states occur at the transition from contraction to dilation, and these states are located on a line, the *Characteristic Line cl*, through the stress origin. The slope of the Characteristic line may be described by an angle, φ_{cl}, (Ibsen and Lade 1998).

Contraction and dilation can be caused by application of shear stresses as well as by changes in the mean normal stress. In the constant p'-test the increment $\delta p'$ is zero and the measured volumetric strains are caused entirely by shear stresses. Since there is no change of p', there in no elastic volumetric strain and the volume change is purely plastic. In elasto-plasticity models the characteristic state, evaluated from $p' = const.$ tests, therefore corresponds to the point on the plastic potential surface where the plastic strain increment vector is perpendicular to the p'-axis or the hydrostatic axis, as shown in Figure 1. The characteristic line represents the trace of this point in the stress space and divides it into two subspaces in which the stress combinations lead to different deformation mechanisms.

Below the characteristic line the stress combinations lead to contraction, i.e. $\delta\varepsilon_v^p > 0$.
Above the line the stress combinations lead to dilation, i.e. $\delta\varepsilon_v^p < 0$.

Below the characteristic line the resistance to deformation is governed by sliding friction due to microscopic interlocking depending upon surface roughness of the particles or interlocking friction between particles. The resistance is due to pure friction and the characteristic state describes an intrinsic parameter, which defines a characteristic angel φ_{cl} for a given sand. This angle is independent of the relative density I_D , as shown in (Lade and Ibsen 1997, Ibsen and Lade 1998).

3.2 Interlocking capacity

Luong (1982) defined the characteristic state in a similar manner, as described above, based on conventional triaxial compression tests. In conventional triaxial tests, where the confining pressure is constant, the stress path corresponds to $\delta q'/\delta p' = 3$. Luong's characteristic state will in the following be refereed to as the *Interlocking Capacity State* of the sand.

The volumetric strain curves from three triaxial tests on Aalborg University sand No. 1 conducted with different stress paths are shown in Figure 4. The tests were all performed on specimens with I_D = 1.00 and consolidated to a mean normal stress of p' = 200 kPa before shearing.

In the constant p'-test the volumetric strains are caused entirely by shear stresses. The test shows shear-induced contraction in the beginning, and it is possible to define a characteristic state, as shown in Figure 4. As expected, the contraction becomes more pronounced as the stress ratio $\delta q'/\delta p'$ decreases, and there are distinct differences between the characteristic states obtained from different stress paths. In Figure 5 the characteristic state and the interlocking capacity states, evaluated from the

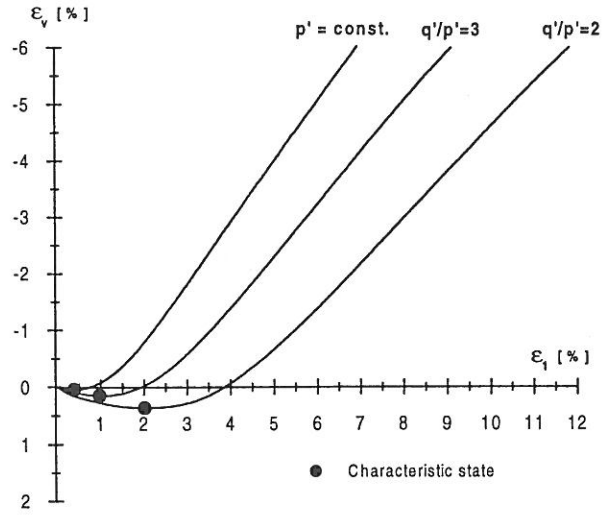

Figure 4. Volumetric curves obtained by stress path tests on Aalborg University sand No. 1. I_D = 1.00. Isotropic consolidated to p'= 200 kPa before shearing.

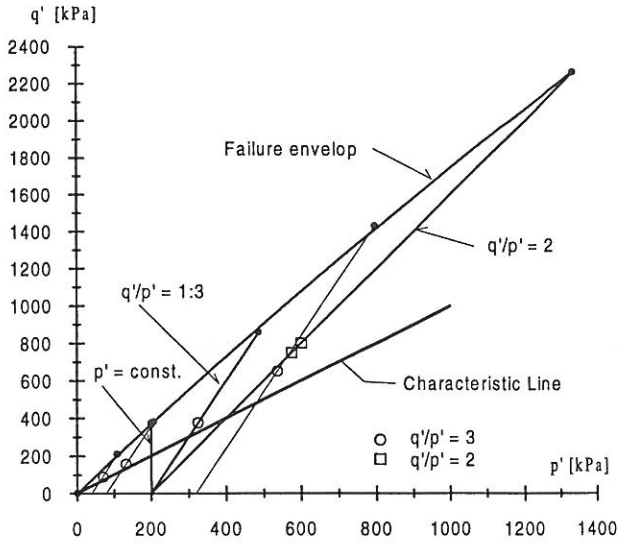

Figure 5. Stress paths employed in triaxial compression tests on Aalborg University sand No 1, I_D= 1.00

test with the stress path $\delta q'/\delta p' = 3$ $\delta q'/\delta p' = 2$, are compared. The figure shows, that the interlocking capacity states are located above the characteristic line and the values increase with decreasing stress path. For different stress paths, the increment in p', produces both an elastic and plastic volumetric strain increment. The plastic volumetric strain is defined by the particular combination of stresses at the particular point where the characteristic line is reached, and not by the stress path followed. Whereas, the elastic volumetric strain is a function of the stress path followed. The distinction between the characteristic and interlocking capacity state is the elastic volumetric strain increment included in the interlocking capacity state. The interlocking capacity state is therefore stress path dependent and not useful as an intrinsic parameter in elasto-plasticity models.

3.3 Comparison of phase transformation and characteristic stress states

The phase transformation stress state plays a similar role for undrained tests as the characteristic stress state plays for drained tests. Figure 6 shows a schematic illustration of the stress state at which phase transformation occurs along an effective stress path from an undrained test. It is the point at which "the stress path turns its direction in p'- q' space" (Ishihara et al. 1975), i.e. the point where the effective stress path has a "knee" and the effective mean normal stress reaches a minimum value p'_{min}.

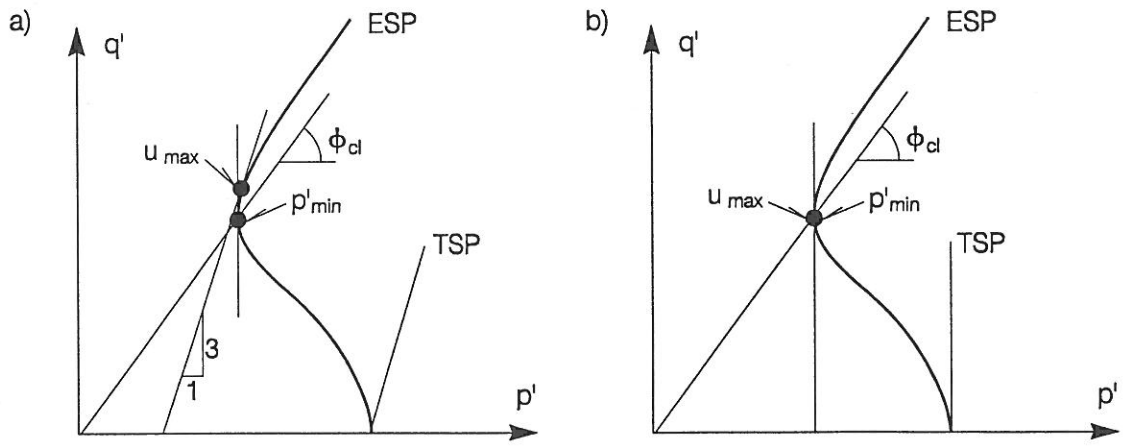

Figure 6. Schematic diagram of phase transformation state in undrained triaxial compression tests on sand. a) Conventional total stress path $\delta q'/\delta p' = 3$, b) Total stress path $p = const.$

Whereas the "knee" described above does not clearly define the location of the phase transformation point, the most consistent definition is one that is independent of the stress path. The phase transformation state is therefore best defined as the point at which the effective stress path has a vertical tangent.

At this point of the undrained test, the increment $\delta p'$ becomes zero, and the elastic volumetric strain increment, $\delta\varepsilon_v^e$, is therefore also zero. Consequently, the plastic volumetric strain increment, $\delta\varepsilon_v^p$, is also zero. This definition theoretically makes the characteristic and phase transformation states identical, (Ibsen and Lade 1998).

3.4 Comparison of critical state and characteristic stress states

Different versions of the conditions that constitute critical state have been presented in the literature (Casagrande 1940, Seed and Lee 1967). These are illustrated in Figure 7 together with the definition of the characteristic state, (Ibsen and Lade 1998).

According to Casagrande (1940), critical state is reached under drained conditions when the void ratio and the normal and shear stresses remain constant under continued shearing. In sands, critical state typically occurs after peak failure at large strains, as illustrated in figure 7. Reaching critical state under undrained conditions would require that the pore pressure and the effective stresses remain constant at large strains.

Seed and Lee (1967) defined critical state as the combination of void ratio, after consolidation, and confining pressure that produces zero total volume change at peak failure under drained conditions, as also illustrated in Figure 7. The critical state line obtained according to Seed and Lee's definition is different from that obtained at large strains, especially for low void ratios and high confining pressures. Today the term critical state refers to the Casagrande's defined critical state.

The characteristic state and the critical state are very similar, as discussed by (Luong 1982). For loose sand and sand at high confining pressure, $\delta\varepsilon_v/\delta\varepsilon_1 = 0$ is reached at the critical state. The critical state is therefore the same as the characteristic state, and it occurs at failure for sand that compresses during shear. For dense sand or sand at low confining pressure, the characteristic state is reached at small strain magnitudes, as indicated in Figure 7, while the critical state is reached at large strains. The effect of post-peak shear banding in drained triaxial compression tests on dense, medium and even loose sands and nonuniformity of specimen geometry at large axial strains, all affect the overall determination of Casagrande's critical state. In addition, evaluating experimental results to determine when critical state occurs is difficult, because rarely do the stress and

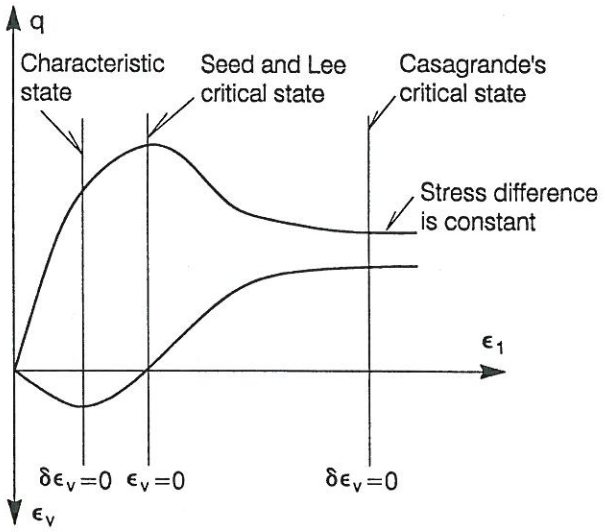

Figure 7. Comparison of phase transformation and characteristic stress states.

volume change tendencies in a specimen remain constant for very long. Contrary to this, the characteristic state is defined pre-peak under uniform stress and strain condition. The state is well defined, and the evaluating of the experimental results to determine when the characteristic state occurs is easy. Compared to the critical state, the characteristic state is much more suitable as an intrinsic parameter in elasto-plasticity models.

4 CHARACTERISTIC STATE AND STATIC SAND BEHAVIOUR

4.1 Drained shear strength of sand

The typical variation of drained shear strength of sand with mean effective stress is illustrated schematically in Figure 8. For a sand with a given initial density, the peak friction angle consists of two components. One from the basic friction between sand

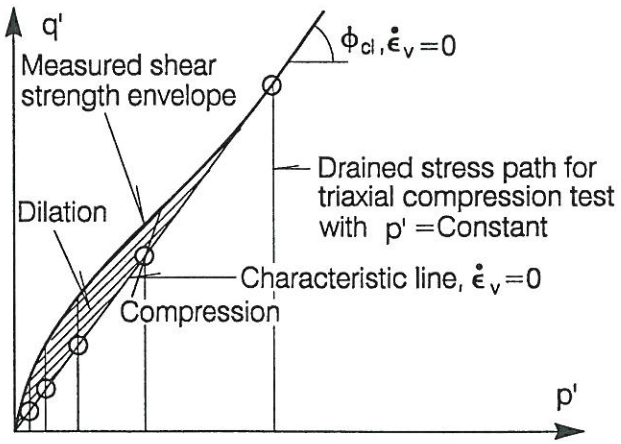

Figure 8. Variation of drained shear strength envelope for sand with mean normal pressure.

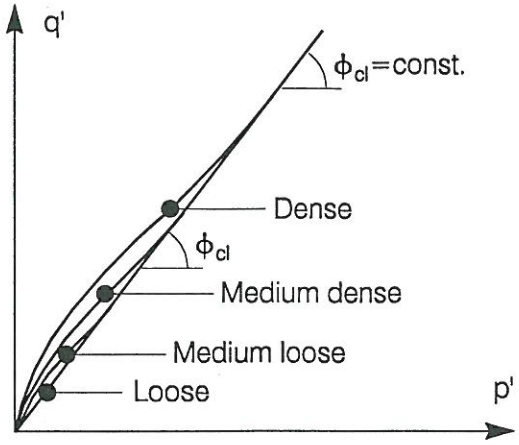

Figure 9. Variation of drained shear strength envelope for sand with relative density.

particles modified for contributions from rearrangement of particles at constant volume. The resulting friction angle is referred to as the characteristic friction angle φ_{cl}.

The second component derives from the dilation of the sand during shear. The dilation is suppressed at higher pressures due to crushing, and the resulting strength component therefore reduces to zero at very high pressures. Thus, a curved failure surface is observed. In this subspace, situated between the failure envelope and the characteristic line, the resistance to deformation is governed by interlocking disrupture. The individual particles are plucked from their interlocking seats and made to slide over/around the adjacent particles leading to large dilative volumetric changes. The resistance to the deformation and thereby the size of the subspace is strongly dependent on the initial sand density. It requires more energy for the grains in a dense sand to move the adjacent particles, than for the grains in a loose sand. The subspace does not exist in a very loose sand where no dilation occurs and in this case the failure envelope will be identical to the characteristic line. Experiments on sands have shown that both the contribution from dilation and the range of confining pressures in which dilation occurs reduce with decreasing relative density, as shown schematically in Figure 9.

4.2 Undrained shear strength of sand

The three schematic stress paths shown in Figure. 10 represent the three types of undrained behaviour typically observed for clean sands, (Yamamuro and Lade 1997).

Results of four conventional undrained triaxial tests performed at low pressure are shown in Figure 11. During undrained shear at low pressure, the pore pressure increases at first in order to prevent the sand from contraction, i.e. $\delta u > 0$. When the deviator stress approaches the characteristic state $\delta p' \rightarrow 0$. The test in Figure 11, indicates that the stress states where $\delta p = 0$ are located on the characteristic line. If q' is increases further, the effective stress path is located in the subspace which is characterised by dilation. In order to prevent dilation, the pore pressure generation becomes negative, i.e. $\delta u < 0$, as shown in Figure 11.a. This directs the stress path to the right towards higher effective confining pressures, causing the stress difference to increase continuously towards the point where the characteristic line and the drained failure envelope merge and become identical, as shown in Figure 10. At that point, failure develops. Figure 11.a shows that the effective stress path approaches a common stress path asymptotically, defined by the stress stage marked with open squares. This common stress path is identical with the stress path defined by the stress states where $\Sigma \delta \varepsilon_v = 0$, marked by open squares in figure 3.

This common stress path is normally considered to be the undrained failure envelope. In figure 11.b it is shown that the common stress path does not represent any failure in the sand, and tests covering a σ'_3 interval from 5 to 2000 kPa do not reveal any maximum at the performance curves. The sand behaviour is entirely stable until the point is reached, where the characteristic line and the drained failure envelope become identical

If the effective stress paths are studied in detail, it is observed that the stress state corresponding to maximum pore water pressure u_{max} occurs slightly later than the characteristic stress state, as indicated in Figure 6.a. If the tests are performed as undrained test, where the total stress path TSP p is constant, it is observed that the stress state corresponding to maximum pore water pressure u_{max} is identical with the characteristic stress state, as shown in Figure 6.b. Along the effective stress path in Figure 6.b, the elastic and plastic volumetric strains have to

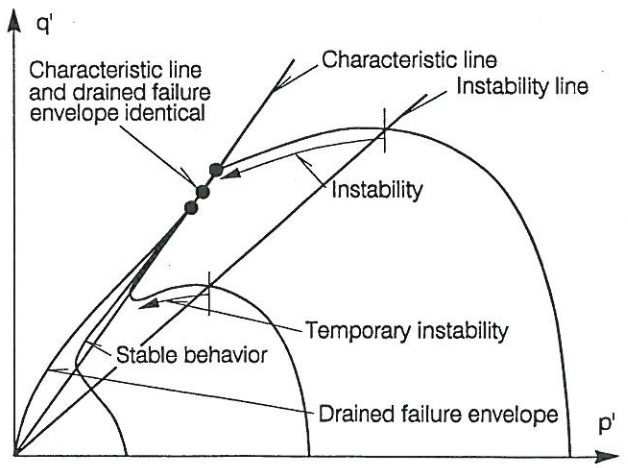

Figure 10. Schematic stress paths of undrained soil behaviour.

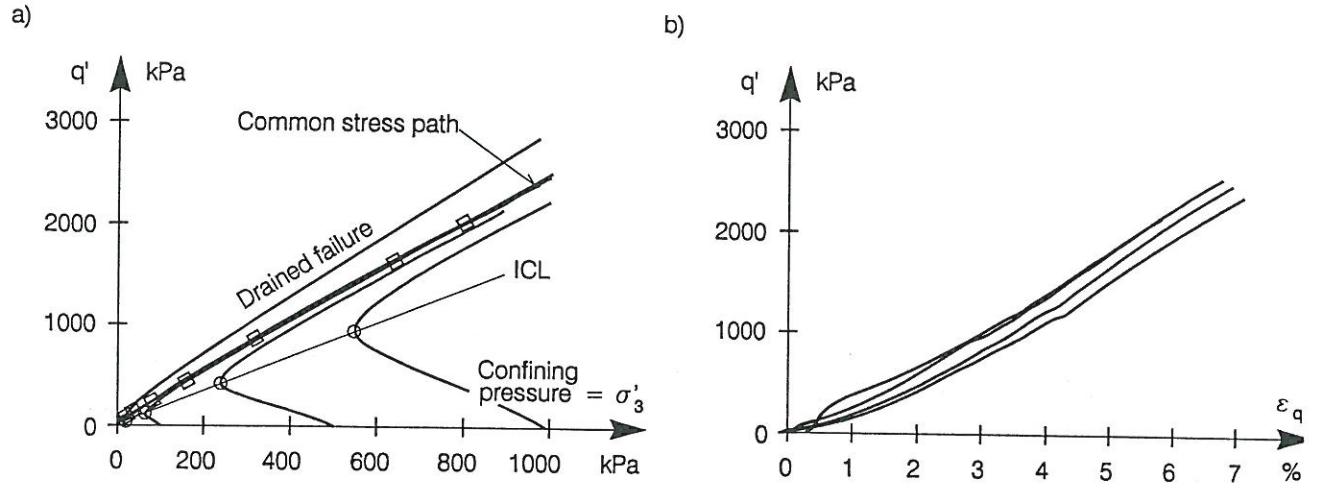

Figure 11. Results of four undrained tests performed on Lund sand No. with $I_D = 0.78$.

compensate for each other, i.e. $\varepsilon_v^e = -\varepsilon_v^p$. Since there is no change in the mean normal stress p', there is no elastic volumetric strain either, i.e. there is no change in the amount of elastic strain energy stored in the soil. The stress state corresponding to maximum pore water pressure u_{max} is therefore identical with the characteristic stress state.

In the conventional undrained compression test, see figure 6.a, the total stress path corresponds to $\delta q/\delta p = 3$ and additional elastic energy is stored in the soil. The elastic volumetric strain is identical with what was observed in the drained tests under the effective stress path $\delta q'/\delta p' = 3$. The stress state corresponding to maximum pore water pressure u_{max}, is therefore identical with the interlocking capacity of the soil. For an arbitrary total stress path, different from constant p, the interlocking capacity controls the stress point where the maximum pore water pressure u_{max} occurs. This stress point is therefore also stress path dependent.

The middle stress path in Figure. 10, indicates a more contractive behaviour pattern experienced at medium high confining pressures. The distance between the instability line and the characteristic line, is so large that the effective stress path is able to "wrap around" the top of the plastic yield surface. Then loading can occur while all stresses are decreasing (Lade 1992). The undrained sand behaviour along this declining portion of the effective stress path is unstable in the sense that the sand cannot sustain the current stress difference. However, as the effective stress path crosses the characteristic line, the suppressed dilation produces negative pore pressure increments, and the effective stress path is consequently directed towards higher effective confining pressures and higher stress differences. This stable behaviour continues until the point where the characteristic line and the drained failure envelope merge is reached. Thus, temporary instability is observed in the middle ranges of confining pressure (Yamamuro and Lade 1997). Note that the point where the characteristic line and the drained failure envelope become identical does not coincide, because the void ratio after consolidation decreases with increasing confining pressure causing the failure envelope to grow, as shown in figure 10. The end points will therefore be slightly different for tests consolidated to difference confining pressures.

The third effective stress path at the highest confining pressure in Figure 10 indicates large contractive tendencies resulting in continuously increasing pore pressures. The effective stress path reaches a peak at the instability line, after which it declines until the characteristic line is reached. The characteristic line is reached at a stress level where the characteristic line and the drained failure envelope are identical. In this case the effective confining pressure is so high that there is no tendency for dilation. Past the point of maximum stress difference, the undrained sand becomes unstable (Lade et al. 1988, Lade 1993, Yamamuro and Lade 1997). This unstable behaviour continues until the point where the characteristic line and the drained failure envelope merge is reached. The stress difference and the mean stress stabilises, but failure develops completely.

4.3 Static liquefaction

The term static liquefaction is used for the condition described by $\sigma_3' = 0$ and $\sigma_1 - \sigma_3 = 0$. Static liquefaction can only develop in very loose sand at low confining pressure. In this situation, the third effective stress path in figure 10 is observed. As a consequence of the applied confining pressures, a small subspace, where the soil dilate will always exist. The point where the characteristic line and the drained failure envelope merge will always exist. The declining stress will therefore stabilise before the static liquefaction is reached. An accelerator is needed to overcome this point in order to develop static liquefaction. The accelerator is the additional

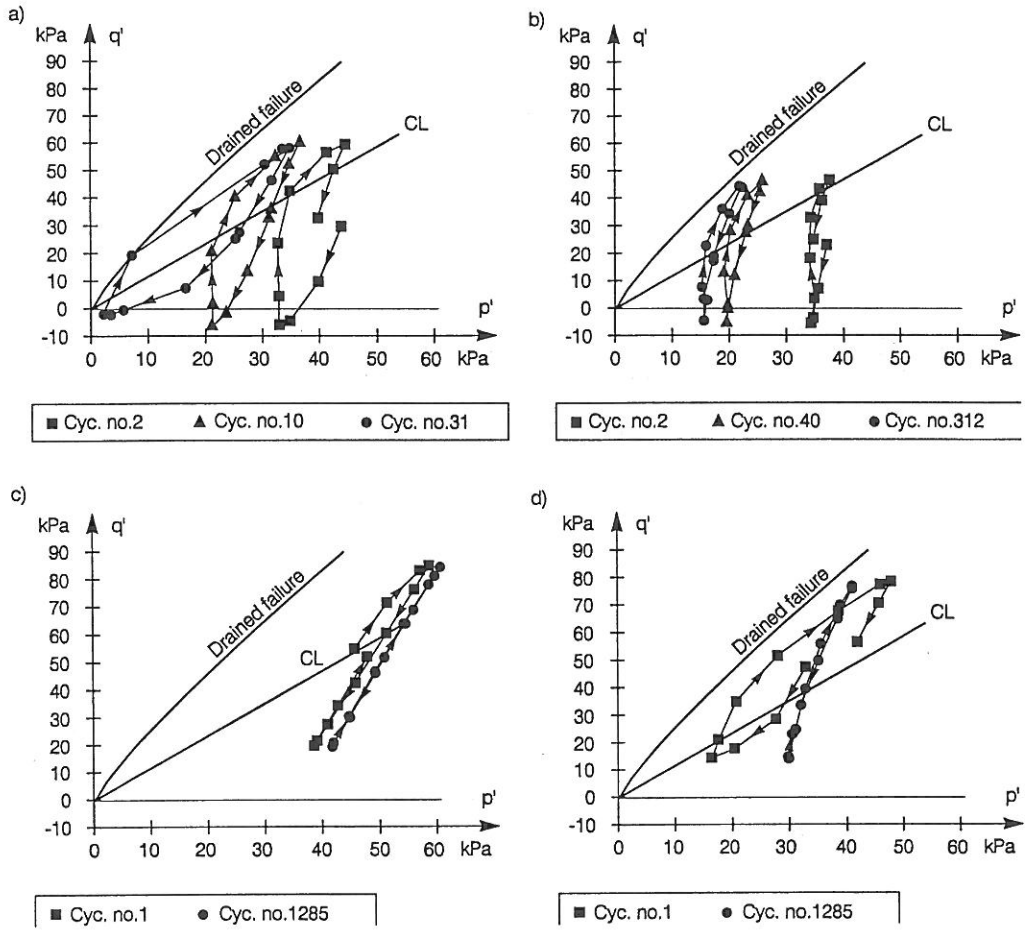

Figure 12. Outline of the phenomena observed in cyclic triaxial tests. a) cyclic liquefaction, b) pore pressure buildup, c) stabilisation, d) instant stabilisation.

elastic energy stored in the soil, i.e. the difference between the characteristic and the interlocking capacity, as described above. The elastic energy is both material and stress path dependent. It's potential is relative small and it can only accelerate the declining stresses so static liquefaction is developed at very low confining pressures, as shown by (Yamamuro and Lade 1997).

5 THE CHARACTERISTIC STATE AND CYCLIC LOADING

Liquefaction is more likely to occur under cyclic loading than during static loading. In the case of undrained cyclic loading the stress variation can develop cyclic liquefaction even at very dense densities. The cyclic failure condition, such as cyclic liquefaction (Seed and Lee 1966) and Cyclic Mobility (Casagrande 1971) is only part of the complex mechanism, which has to be determined in order to describe the development of stress and strain in cyclic tests. Experiments have been performed to study the factors that influence and control the fatigue which leads to Cyclic Liquefaction. (Ibsen 1993). The observed stress paths, can be divided in four typical stress paths, as shown in Figure 12. Two typical stress path in which positive pore pressures are generated. The phenomena named *Pore Pressure Buildup* or *Cyclic Liquefaction* can be observed. These stress paths are shown in Figure 12 a) and 12 b), and two typical stress paths in which negative pore pressures are generated. The phenomena named *Stabilization* or *Instant Stabilization* can be observed. These stress paths are shown in Figure 12 c) and 12 d). These four typical stress paths will be shown to be controlled by the characteristic state.

5.1 Drained cyclic loading

In Figure 13 cycling sequences are carried out at different deviator stress levels under drained conditions and at constant confinement, $\sigma_3' = 200$ kPa. Each cycling sequence consists of 20 cycles with an amplitude of 100 kPa. The diagram shows very clearly that the contracting behaviour of the soil is obtained when the mean deviator stress level is lower than the characteristic level at the interlocking capacity state. The dilation behaviour of the soil during load cycling is evident when the mean deviator stress level becomes higher than the characteristic threshold, q'_{cl}.

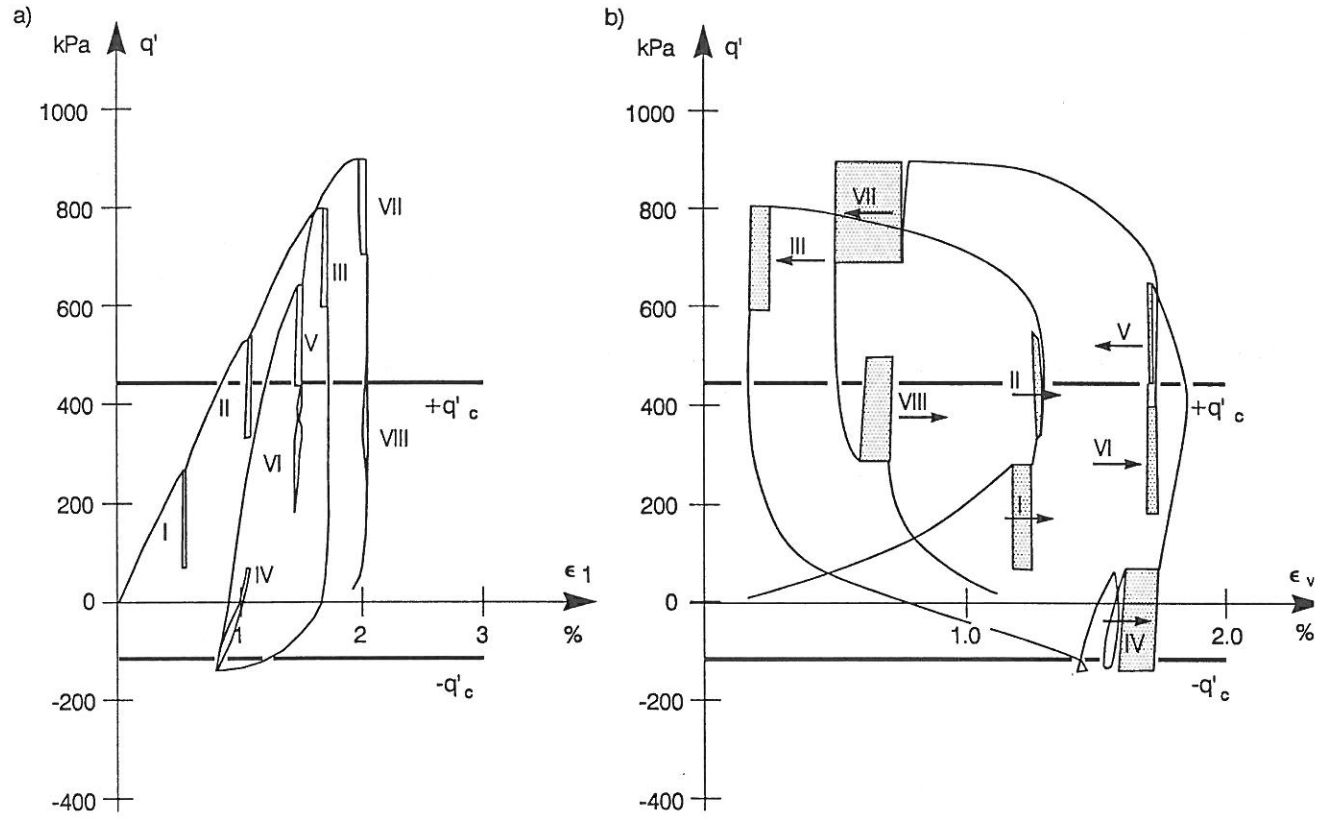

Figure 13 Cyclic loading under constant confining pressure 200 kPa performed on Fountainbleau sand I_D = 0.64 (data from Luong 1982).

5.2 Undrained cyclic loading

Similar to the drained cyclic test in Figure 13, and with the experience from the static test in mind, the interlocking capacity state could then be expected to control pore pressure in the soil during conventional undrained cyclic loading. However, the changes in the effective stress path due to cyclic loading are composed of the pore pressure produced during the loading part of the cycle and the changes in the pore pressure during the unloading part of the cycle. In Ibsen (1994) the interlocking capacity state was shown only to control the changes in the pore pressure during the loading part of the cycle. Therefore, the interlocking capacity state is not able to control the stress hardening/softening of the soil during a complete cycle.

It is assumed that a stress state exists, where the positive and negative pore pressures generated during a loading cycle neutralise each other. The stress state is defined as $\Sigma \delta u = 0$ during a cycle. The stress state is described as the *Cyclic Stable State.* Each time the mean deviator stress level is lower than the cyclic stable state positive pore pressure will be generated and negative pore pressure is generated each time the mean deviator stress level becomes higher. As a consequence the cyclic loading leads the mean normal stress towards the cyclic stable state in each test, as shown in figure 14, and when the cyclic stable state has been reached the mean normal stress

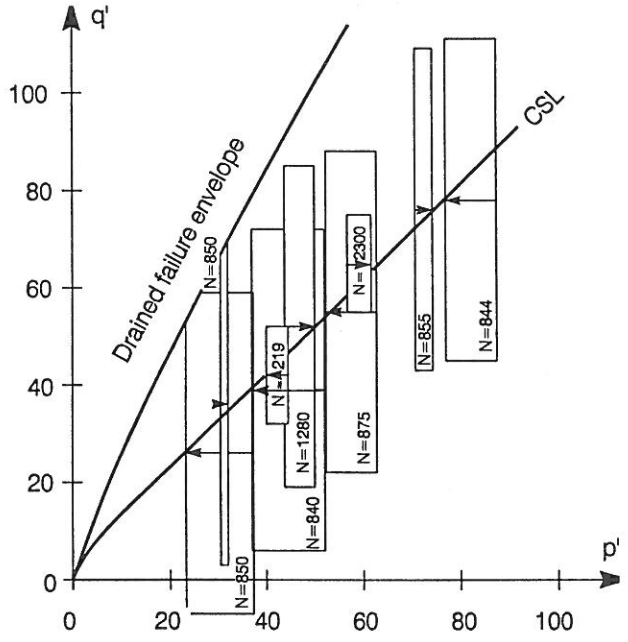

Figure 14. The effective stress path of nine cyclic test is shown. The test is performed on Lund No. 0 with I_D = 0.78 and on specimens with equal height and diameter. N is the number of cycles added to the test and the arrow describes the changes in the effective mean stress.

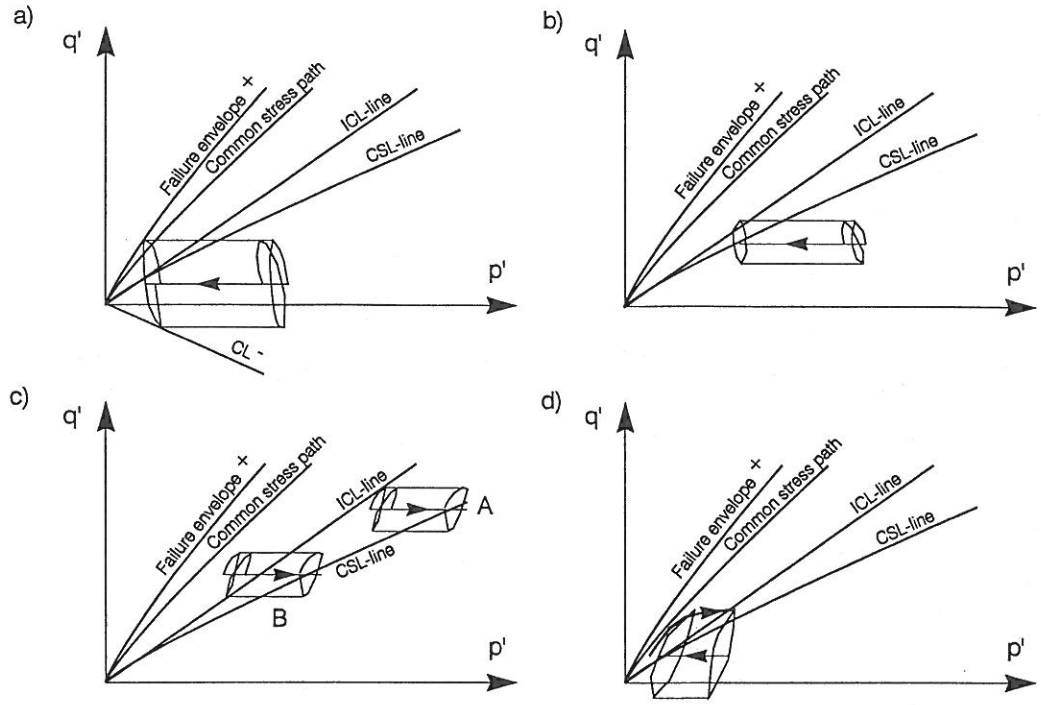

Figure 15 Observed phenomena explaned by the cyclic fatigue theory for sand

does not change and the cyclic loading will not lead to further hardening or softening of the soil.

5.3 The cyclic fatigue theory for sand

The drained stress state (p'_s, q'_s), present before the cyclic loading is added to the test, controls the variation of the effective mean stress. If the anisotropic mean stress level is situated below the characteristic line CL, the increase in pore pressure during the loading part of one cycle is greater than the reduction during the unloading part. The cyclic loading will then lead to pore pressure buildup and the effective normal stress will decrease , as shown in Figure 15. a) and 15. b.

Failure can take place, if the minimum stress level after a number of cycles exceeds the characteristic line in extension CL$^-$. The pore pressure generation δu will then go from $\delta u > 0$ to twice during each cycle and the equilibrium of the stable state cannot be created. After the minimum stress level q'_{min} has exceeded the characteristic line in extension CL, the drained failure envelope will be reached during the subsequent cycle. Cyclic Liquefaction as defined by Casagrande (1971) will be observed if the maximum stress level q'_{max}during the subsequent cycle reaches the drained failure envelope in compression. Necking, which is a phenomenon similar to Cyclic Liquefaction and defined by Casagrande (1971) will be observed if q'_{min} reaches the drained failure envelope in extension. This failure mechanism is outlined in Figure 15 a). If the cyclic stable state is developed during the cyclic loading no failure will occur and the phenomenon Pore Pressure Buildup will be observed, as shown in figure 15. b). According to the figure no further changes in the mean normal stress will be observed while adding further cycles.

If the anisotropic mean stress level is situated above the stable line CSL, the cyclic loading will generate negative pore pressure. Similar to the phenomenon Pore Pressure Buildup the cyclic stable state can be developed during the negative pore pressure generation and the phenomenon Stabilization will be observed, as shown in Figure 15.c). If the amplitude of the cyclic load is so large that the stress variation during the first half cycle follows the common stress path, the mean stress level changes from being situated above the cyclic stable line to being situated below, as shown in Figure 15.d). After the first half cycle, where considerably negative pore pressure is generated, the cyclic loading will generate positive pore pressure due to the fact that the mean normal stress state is situated below the stable line. The phenomenon which is described as Instant Stabilization will be observed. Similar to Pore Pressure Buildup failure can take place, if the minimum stress level q'_{min} after a number of cycles exceeds the characteristic line in extension CL$^-$, otherwise the Stable State will develop.

6 CONCLUSIONS

Studying the basic sand behaviour in triaxial tests under uniform conditions, similar responses of the sand due to static and cyclic loading have been discovered. The static and cyclic responses of sand can

be explained with help of the characteristic state, and the strength of sand under undrained conditions is found to be controlled by the drained failure condition for both static and cyclic loading.

In this paper, the characteristic state is redefined as the stress state where $\delta\varepsilon_v$ becomes zero for the first time in a constant p' test. Further, the phase transformation state is defined as the state where becomes zero for the first time. As a consequence, the characteristic and phase transformation lines become identical. These definitions are mutually consistent, and they may therefore be useful in controlling the plastic potential function for description of plastic volume changes of soils.

In comparison, the characteristic angle defined by Luong (1982) is not an intrinsic parameter, independent of stress path, and it not useful for development of elasto-plasticity models.

Performing cyclic triaxial tests on specimens, which ensure homogeneous stress and strain distribution throughout the test, the existence of a cyclic stable state is found. The cyclic stable state is shown to have a considerable influence on the development of the effective stress variations during cyclic loading. The cyclic stable state represents an ideal stress state, where the positive and negative pore pressures generated during a loading cycle neutralise each other, and the mean normal stress is shown not to change, when the stable state is reached, and further loading will not lead to any stress hardening or softening of the soil. The cyclic stable state is an intrinsic parameter, which is found to be independent of the amplitude of the cyclic load.

The cyclic stable state is shown to divide the stress space into two subspaces, where the cyclic loading will generate positive or negative pore pressures, respectively. Especially the new phenomena Stabilization and Instant Stabilization observed in connection with the development of negative pore pressure are of great interest.

7 REFERENCES

Casagrande, A. 1971. On Liquefaction phenomena. *Geotechnique,* September, 1971 XXI(3), 197-202.

Guzmann, A. A. et al. 1988. Undrained monotonic and cyclic strength of sand. *Journal of the Geotechnical Engineering Division ASCE,* 114(10), 1089-1118.

Ibsen, L.B. 1994. The stable state in cyclic triaxial testing on sand. *Soil Dynamics and Earthquake Engineering 13,* 63- 72.

Ibsen, L.B 1993 Poretryksopbygning i sand. (Pore perssures in sand). *Ph.D Thesis.* Soil Mechanic Laboratory, Aalborg University, Denmark , Jan. 1993.

Ibsen, L.B. and Bødker, L. 1994. Baskarp Sand No. *15. Data Report 9301,* Soil Mechanics Laboratory, Aalborg University, Denmark.

Ibsen, L.B and Lade P.V. 1998. The Role of the Characteristic Line in Static Soil Behavior. *4" Workshop on Localisation and Bifurcaton Theory for Soils and Rocks*, A. A Balkema.

Ibsen. L.B. and Jakobsen, F.R. 1996. Lund Sand No. 0, *Data Report 8401, 8402, 8801 & 8901,* Soil Mechanics Laboratory, Aalborg University, Denmark.

Ishihara, K., Tatsuoka, F. and Yasuda. S. 1975. Undrained deformation and liquefaction of sand under cyclic stresses. *Soils and Foundations,* 15(1),29-44.

Jacobsen, M. 1970. New Oedometer and Triaxial Apparatus for Firm Soil. *DGI Bulletin No. 27.*

Jakobsen, F.R. and Simonsen, J. 1994 Horizontal resistance of dynamically loaded piles. (in Danish). *MSc. Thesis.* Aalborg University.

Lade, P.V. 1992. Static Instability and Liquefaction of loose fine sandy slopes. *Journal of Geotechnical Engineering, ASCE, 118(1),* 51-71.

Lade, P.V. 1993. Initiation of static instability in the submarine Nerlerk berm, *Canadian Geotechnical Journal*, 30(6) ,895-904.

Lade, P.V. 1994. Instability and Liquefaction of granular materials. *Computers and Geotechnics*, 16, 123-151.

Lade,P.V. 1995. Instability of sand in the prefailure hardening regime. *Proc. First conf on pre-failure Deformation Characteristics of Geomaterials*, 2:837-854.

Lade P.V, Nelson,R.B., and Ito,Y.M (1988). Instability of granular materials with nonassociated flow, *Journal of Engineering Mechanics*, ASCE, 114 (12),2173-2191.

Lade P.V and Ibsen L.B 1997. A Study of the Phase Transformation and the Characteristic Lines of Sand Behavior. *Deformation and Progressive failure in Geomechanics. IS-NAGOYA '97.* Pergamon Press, 353-358.

Lade, P.V. and Prabucki, M.-J. 1995. Softening and preshearing effects in sand. *Soils and Foundations,* 35(4), 93-104.

Luong, M.P. 1982. Stress-strain aspects of cohesionless soils under cyclic and transient loading. *International Symposium on Soil under Cyclic and transient Loading,* A. A Balkema, Rotterdam, 3 15-324.

Seed, H.B. and Lee, K.L. (1967).Undrained strength characteristics of choesionless soil,*Journal of Soil Mechanics and Foundations Division,* ASCE, 93(6), 333-360.

Yamamuro J.A. and Lade P.V. 1997. Static liquefaction of very loose sand. *Canadian Geotechnical Journal* 34, 905 - 917.

AGEP: Soil Mechanics papers

6 Ibsen, L.B. (1995). Soil Parameters, Final proceedings MCS - Project MAST II, July 1995. Also in *AAU Geotechnical Engineering Papers*, ISSN 1398-6465 R9514.

7 Sørensen, C. S., Ibsen, L. B. , Jakobsen, F. R., Hansen, A., Jakobsen, K. P., (1995) "Bearing Capacity of Caisson Breakwaters on Rubble Mounds". Proceedings of the Final Project Workshop, Monolithic (Vertical) Coastal Structures, Alderney, UK, Appendix IX, p 26. Also in *AAU Geotechnical Engineering Papers*, ISSN 1398-6465 R9515.

8 Ibsen, L.B., Steenfelt, J.S. (1996). Terningapparatet - et middel til bedre jordforståelse (The true-triaxial-apparatus - a means to better understanding of soil behaviour; in Danish). *Proc. Nordic Geotechnical Meeting, NGM-96, Reykjavik,* Vol 1, pp 111-122. Also in *AAU Geotechnical Engineering Papers*, ISSN 1398-6465 R9603.

9 Thorsen, G., Thomsen, B., Thorsen, S. (1996). Tilsyneladende forbelastning af Eem jordarter (Apparent preconsolidation of Eemian soils; in Danish). *Proc. Nordic Geotechnical Meeting, NGM-96, Reykjavik*, Vol 1, pp 147-152. Also in *AAU Geotechnical Engineering Papers*, ISSN 1398-6465 R9607.

10 Thorsen, G. (1996). Oedometer tests - an aid in determination of the geological load history. *Bull. of the Geological Society of Denmark*, Vol. 43, pp. 41-50. Copenhagen 1996-07-14. Also in *AAU Geotechnical Engineering Papers*, ISSN 1398-6465 R9608.

11 Ibsen, L.B., Jakobsen, K.P. (1997). Dynamic Bearing Capacity of Caisson Breakwaters Subjected to Impulsive Wave Loading. MAST III (PROVERBS Workshop, Las Palmas, Feb. 18-24-1997. Also in *AAU Geotechnical Engineering Papers*, ISSN 1398-6465 R9701.

12 Lade, P.V., Ibsen, L.B. (1997). A study of the phase transformation and the characteristic lines of sand behaviour. Proc. Int. Symp. on Deformation and Progressive Failure in Geomechanics, Nagoya, Oct. 1997, pp. 353-359. Also in *AAU Geotechnical Engineering Papers*, ISSN 1398-6465 R9702.

13 Bødker, L., Steenfelt, J.S. (1997). Vurdering af lodrette flytningsamplityder for maskinfundament, Color Print, Vadum (Evaluation of displacement amplitudes for printing machine foundation; in Danish). *AAU Geotechnical Engineering Papers*, ISSN 1398-6465 R9706.

14 Ibsen, L.B., Steenfelt, J.S. (1997). Vurdering af lodrette flytningsamplityder for maskinfundament Løkkensvejens kraftvarmeværk (Evaluation of displacement amplitudes for gas turbine machine foundation; in Danish. *AAU Geotechnical Engineering Papers*, ISSN 1398-6465 R9707.

15 Steenfelt, J.S. (1997). National R&D Report : Denmark. *Seminar on Soil Mechanics and Foundation Engineering R&D*, Delft 13-14 February 1997. pp 4. Also in *AAU Geotechnical Engineering Papers*, ISSN 1398-6465 R9708.

16 Lemonnier, P. and Soubra, A. H. (1997). Validation of the recent development of the displacement method - geogrid reinforced wall. *Colloquy EC97 on the comparison between experimental and numerical results*, Strasbourg, France. Vol.1, pp. 95-102. Also in *AAU Geotechnical Engineering Papers*, ISSN 1398-6465 R9712.

AGEP: Soil Mechanics papers

17 Lemonnier, P. & Soubra, A. H. (1997). Recent development of the displacement method for the design of geosynthetically reinforced slopes - Comparative case study. *Colloquy on geosynthetics, Rencontres97, CFG*, Reims, France, Vol. 2, pp. 28AF-31AF (10pp). Also in *AAU Geotechnical Engineering Papers*, ISSN 1398-6465 R9713.

18 Lemonnier, P., Soubra, A. H. & Kastner, R. (1997). Variational displacement method for geosynthetically reinforced slope stability analysis : I. Local stability. Geotextiles and Geomembranes 16 (1998) pp 1-25. Also in *AAU Geotechnical Engineering Papers*, ISSN 1398-6465 R9714.

19 Lemonnier, P., Soubra, A. H. & Kastner, R. (1997). Variational displacement method for geosynthetically reinforced slope stability analysis : II. Global stability. Geotextiles and Geomembranes 16 (1998) pp 27-44. Also in *AAU Geotechnical Engineering Papers*, ISSN 1398-6465 R9715.

20 Ibsen, L.B. (1998). Analysis of Horizontal Bearing Capacity of Caisson Breakwater. 2nd PROVERS Workshop, Napels, Italy, Feb. 24-27-98. Also in *AAU Geotechnical Engineering Papers*, ISSN 1398-6465 R9802.

21 Ibsen, L.B. (1998). Advanced Numerical Analysis of Caisson Breakwater. *2nd PROVERS Workshop*, Napels, Italy, Feb. 24-27-98. Also in *AAU Geotechnical Engineering Papers*, ISSN 1398-6465 R9803.

22 Ibsen, L.B., Lade P.V. (1998). The Role of the Characteristic Line in Static Soil Behavior. *Proc. 4th International Workshop on Localization and Bifurcation Theory for Soil and Rocks*. Gifu, Japan. Balkema 1998. Also in *AAU Geotechnical Engineering Papers*, ISSN 1398-6465 R9804.

23 Ibsen, L.B., Lade, P.V. (1998). The Strength and Deformation Characteristics of Sand Beneath Vertical Breakwaters Subjected to Wave Loading. 2nd PROVERS Workshop, Napels, Italy, Feb. 24-27-98. Also in *AAU Geotechnical Engineering Papers*, ISSN 1398-6465 R9805.

24 Steenfelt, J.S., Ibsen, L.B. (1998). The geodynamic approach - problem or possibility? Key Note Lecture, *Proc. Nordic Geotechnical Meeting, NGM-96, Reykjavik, V*ol 2, pp 14. Also in *AAU Geotechnical Engineering Papers*, ISSN 1398-6465 R9809.

25 Lemonnier, P., Gotteland, Ph. and Soubra, A. H. (1998). Recent developments of the displacement method. *Proc. 6th Int. Conf. on Geosynthetics. Atlanta, USA*, Vol 2, pp 507-510. Also in *AAU Geotechnical Engineering Papers*, ISSN 1398-6465 R9814.

26 Praastrup, U., Jakobsen, K.P., Ibsen, L.B. (1998). On the choice of strain measures in geo-mechanics. 12th Young Geotechnical Engineers Conference, Tallin, Estonia. *AAU Geotechnical Engineering Papers*, ISSN 1398-6465 R9815.

27 Ibsen, L.B. (1998). The mechanism controlling static liquefaction and cyclic strength of sand. Proc. Int. Workshop on Physics and Mechanics of Soil Liquefaction, Baltimore. A.A.Balkema, ISBN 9058090388, pp 29-39. Also in *AAU Geotechnical Engineering Papers*, ISSN 1398-6465 R9816.